Modelling of the Fluctuation and Coherent Dynamics in Active Metamaterial Devices

Ming Fang, Zhixiang Huang, *Senior Member, IEEE*, Wei E. I. Sha, *Senior Member, IEEE*, and Costas M. Soukoulis

***Abstract*—Active metamaterials, i.e., coupled systems consist of metamaterials and active or gain media. Modelling the interaction between unconventional electromagnetic response in metamolecules and quantum dynamics of active media in active metamaterials requires the development of a unified and efficient semiclassical model. Here, we propose a semiclassical model based on Langevin Maxwell-Bloch equations and simplified rate equations for a multi-level quantum system. Using the semiclassical model and the finite-difference time-domain (FDTD) algorithm, a methodology for the self-consistent descriptions of both the coherent lasing process and the spatio-temporal spontaneous noise dynamics in active metamaterials is developed. To validate the proposed method, we numerically study the luminescence of QDs hybridized with plasmonic and all-dielectric metasurfaces and compare with the experimental results. The proposed semiclassical method reveals a new approach for developing new types of nanodevices based on active metasurfaces.**

***Index Terms*—Active metamaterials, quantum dot, Maxwell-Bloch theory, quantum noise, all-dielectric metasurface, plasmonic metasurface.**

I. Introduction

RECENT progress in the fields of light-emitting diode (LED), solar cell, laser, and quantum information along with the development of active metamaterials technologies have increased the demand for efficient and unified simulation tools. Specifically, controlling and tuning the stimulated and spontaneous emissions by modulated light-matter interactions in optical metamaterials hybridized with quantum dots (QDs), quantum wells (QWs), and organic dyes has been intensively investigated due to the unconventional electromagnetic properties of the metamaterials [1]–[5]. In this respect, the modelling of spatio-temporal dynamics becomes important for designing and optimizing active metamaterial devices. In addition, for the investigation of active medium interacting with a complex resonant mode of nanocavities, both the spatially inhomogeneous field profile of the cavity mode and the nonlinear dynamics of the atomic system should be precisely captured.

Several approaches have been developed in which the coherent dynamics, spontaneous emissions, and noise fluctuations are rigorously treated in the semiconductor and active medium. A rigorous framework based on the non-equilibrium Green's function formalism was proposed in the early nineties for analysing semiconductor lasers [6]–[8]. The Maxwell-Bloch equations in the second quantization form provide an alternative way for exploiting the interaction of light-matter, the quantum dynamics of the electromagnetic fields and carrier system [9]. Besides, a full quantum mechanical treatment based on a quantum form of the semiconductor Bloch equations (SBEs) and Heisenberg equations has been developed for the study of the interacting electron-hole photon system [10]–[12]. Although these approaches can provide a rigorous framework for modelling the light-matter dynamics, the major drawbacks of these approaches are time-consuming and compute-intensive when a nanocavity with arbitrary geometry is involved. Especially, microscale and nanoscale plasmonic cavities, requiring a three-dimensional description with a deep subwavelength spatial resolution to account for the relevant microscopic processes that affect the semiconductor dynamics due to the drastically inhomogeneous field distribution close to the nanocavities.

We should note that the Maxwell-Bloch equations have been solved by using the finite-difference time-domain (FDTD) method with the incorporations of auxiliary differential equations (ADE) [13]. This numerical approach has been adopted mostly to get spatiotemporal dynamics of semiclassical problems such as semiconductor lasers and amplifiers [14]–[19]. It has been successfully validated against experimental results and density matrix theory. However, the dynamics of quantum fluctuations and noise play an important role in light-matter interaction. It has been demonstrated that the quantum mechanical operator dynamics can be derived into a set of classical c-number

Manuscript received November 14, 2020; revised February 28, 2021 and May 11, 2021; accepted June 18, 2021. Date of publication June 24, 2021; date of current version July 23, 2021. This work was supported in part by the National Science Foundation of China (NSFC) under Grants 61901001, 61971001, and U20A20164 and in part by Anhui Province under Grant 1908085QF259. The review of this article was arranged by Associate Editor D. Mencarelli. *(Corresponding author: Ming Fang.)*

Ming Fang and Zhixiang Huang are with the Key Laboratory of Intelligent Computing and Signal Processing, Ministry of Education, Anhui University, Hefei, Anhui 230039, China, and with the Anhui Province Key Laboratory of Target Recognition and Feature Extraction, Luan, Anhui 237000, China, and with the Institute of Physical Science and Information Technology, Anhui University, Hefei, Anhui 230601, China, and also with the Key Laboratory of Electromagnetic Environmental Sensing, Department of Education of Anhui Province, Hefei, Anhui 230601, China (e-mail: mingfang@ahu.edu.cn; zxhuang@ahu.edu.cn).

Wei E. I. Sha is with the Key Laboratory of Micro-nano Electronic Devices and Smart Systems of Zhejiang Province, College of Information Science and Electronic Engineering, Zhejiang University, Hangzhou 310027, China (e-mail: weisha@zju.edu.cn).

Costas M. Soukoulis is with the Ames Laboratory-U.S. DOE and Department of Physics and Astronomy, Iowa State University, Ames, IA 50011 USA, and also with the Institute of Electronic Structure and Lasers (IESL), FORTH, Heraklion, Crete 71110, Greece (e-mail: soukoulis@ameslab.gov).

Digital Object Identifier 10.1109/TNANO.2021.3092059

Langevin equations for the two-time correlation functions [20]. Slavcheva and Ziolkowski modelled the quantum fluctuations as white Gaussian noise as a source to the electric field in the FDTD simulations of vertical-cavity lasers [21]. Andreasen and Cao developed a numerical model based on the FDTD algorithm to simulate fluctuations in two-level atoms of one-dimensional systems [22]. Pusch *et al.* derived a spatially resolved Maxwell-Bloch Langevin model to describe the light field and noise dynamics in a 3D gain-metamaterial system [23].

In our previous theoretical studies [24]–[28], we established a numerical approach for pump-probe simulations of active semiconductor materials and QDs coupled to plasmonic metamaterials. Based on the Maxwell-Bloch equations, simulations of loss compensation in optical metamaterials with gain medium and lasing spaser based on metamaterials are studied. However, numerical simulation of spontaneous emission cannot be directly captured using this approach. To simulate the spontaneous emission and fluctuations in active medium, we proposed a classical perturbative artificial source model to study spontaneous emission behaviour in the active metasurface based devices [29]. In this paper, the Maxwell-Bloch theory is extended to a Langevin Maxwell-Bloch approach, a spatio-temporal noise dynamic model based on the quantum Langevin equation is linked to simplified rate equations of a multi-level system. The spontaneous emission and noise dynamics can be captured by the Langevin terms, which is a semiquantum picture that can be described as emissions stimulated by vacuum noise. The set of multiphysics equations are self-consistently solved with the help of a 3D ADE-FDTD method. This approach enables us not only to simulate the nanoscale spatio-temporal evolution of electromagnetic fields in a deep subwavelength cavity with arbitrary geometries and material but also includes the noise dynamics in active media. Using examples of pumped plasmonic and all-dielectric metasurfaces with embedded QDs media, we investigate the nonlinear spatiotemporal dynamics and emission spectral characters in active metasurfaces by applying the proposed method. Enhancement and modification of photoluminescence owing to the cavity mode of the metasurfaces are observed and explained by the numerical method.

This paper is organized as follows. In Section II, we introduce the multiphysics model and discuss its numerical solution based on the FDTD method. In Section III, we validate our approach against previous theoretical and experimental studies. We apply our approach to several configurations including QDs embedded in active plasmonic and silicon devices. Potential applications and conclusions of this work are concluded in Section IV.

II. Model and Numerical Implementation

A. Theory and Model

Our starting point is the Maxwell equation for the classical electrodynamics

$$\begin{aligned}\nabla \times \mathbf{E} &= -\partial \mathbf{B}/\partial t \\ \nabla \times \mathbf{H} &= \varepsilon\varepsilon_0 \partial \mathbf{E}/\partial t + \partial \mathbf{P}/\partial t \end{aligned} \tag{1}$$

where $\mathbf{P}$ is the electric polarization density. In general, the polarization can be expressed as $\mathbf{P} = \boldsymbol{\chi}\varepsilon_0\mathbf{E}$, and $\boldsymbol{\chi}$ is the electric susceptibility. $\mathbf{P}$ can be used to associate the Maxwell equations with many multiphysics problems. For example, the equations of Drude model and plasma fluid model can be introduced and coupled to Maxwell's equation by the dynamic polarization. Here, our theoretical consideration for a multi-level atomic system is based on the Maxwell-Bloch equations. A pumped active medium, such as semiconductor QD, coherently absorbs external energy and emits light at a longer wavelength. In order to describe the nonlinear process, a four-level system with two dipole transitions for the absorption process ($0 \leftrightarrow 3$) and the emission process ($1 \leftrightarrow 2$) is required. Two non-radiative transfer processes with short lifetimes ($3 \leftrightarrow 2$) and ($1 \leftrightarrow 0$) are added to couple the two dipole transitions. The equations for the density matrix of the four-level atomic system are given as

$$\begin{aligned}\frac{\partial \hat{\rho}_{12}}{\partial t} &= i\left(\hat{\rho}_{12}\omega_{\mathrm{e}} + \Omega_{12}\left(\hat{\rho}_{11} - \hat{\rho}_{22}\right)\right) - \Gamma_{\mathrm{e}}\hat{\rho}_{12} + \hat{F}_{12} \\ \frac{\partial \hat{\rho}_{03}}{\partial t} &= i\left(\hat{\rho}_{03}\omega_a + \Omega_{03}\left(\hat{\rho}_{00} - \hat{\rho}_{33}\right)\right) - \Gamma_a\hat{\rho}_{03} + \hat{F}_{03} \\ \frac{\partial \hat{\rho}_{00}}{\partial t} &= -2\,\mathrm{Im}\left(\Omega_{03}\hat{\rho}_{03}\right) + \gamma_{10}\hat{\rho}_{11} - P_r\hat{\rho}_{00} + \hat{F}_{00} \\ \frac{\partial \hat{\rho}_{11}}{\partial t} &= -2\,\mathrm{Im}\left(\Omega_{12}\hat{\rho}_{12}\right) + \gamma_{21}\hat{\rho}_{22} - \gamma_{10}\hat{\rho}_{11} + \hat{F}_{11} \\ \frac{\partial \hat{\rho}_{22}}{\partial t} &= 2\,\mathrm{Im}\left(\Omega_{12}\hat{\rho}_{12}\right) - \gamma_{21}\hat{\rho}_{22} + \gamma_{32}\hat{\rho}_{33} + \hat{F}_{22} \\ \frac{\partial \hat{\rho}_{33}}{\partial t} &= 2\,\mathrm{Im}\left(\Omega_{03}\hat{\rho}_{03}\right) + P_r\hat{\rho}_{00} - \gamma_{32}\hat{\rho}_{33} + \hat{F}_{33} \end{aligned} \tag{2}$$

where $\Omega_{12} \equiv \Upsilon_e E/\hbar$ and $\Omega_{03} \equiv \Upsilon_a E/\hbar$ are the Rabi frequencies, Υ_e and Υ_a are the dipole coupling terms, ω_e and ω_a the emission and absorption frequencies. Γ_e and Γ_a are the emission and absorption dephasing rates corresponding to decoherent of the polarization $\hat{\rho}_{12}$ and $\hat{\rho}_{03}$. A simplified homogeneous pump mechanism is used, the external optical pump field is numerically simplified by a homogeneous pumping rate P_r. Thus, the polarization density of the absorption transition is neglected. Following the approach of noise models in the two-level atomic system as presented by Andreasen and Cao, the additional noise terms $\hat{F}$ on the occupation densities and polarization in the four-level system need to be derived from the fluctuation-dissipation theorem.

$$\left\langle \hat{F}_i(t)\hat{F}_j(t)\right\rangle = \left(\frac{d}{dt}\left\langle \hat{A}_i\hat{A}_j\right\rangle\right)_{\mathrm{NH}} - \left\langle \hat{D}_i\hat{A}_j\right\rangle - \left\langle \hat{A}_i\hat{D}_j\right\rangle \tag{3}$$

The subscript <NH> after the bracket denotes that only dissipative terms (non-Hamiltonian) terms are to be included. $\hat{A}$ and $\hat{D}$ are the dynamic operators and dissipation operators. Therefore the stochastic noise terms related to the pumping and dissipation of the atomic density matrix can be calculated from (3)

$$\begin{aligned}\left\langle \hat{F}_{12}\hat{F}_{12}^{\dagger}\right\rangle &= \left(\frac{d}{dt}\left\langle \hat{\rho}_{12}\hat{\rho}_{12}^{\dagger}\right\rangle\right)_{\mathrm{NH}} \\ &\quad + \left\langle \Gamma_e\hat{\rho}_{12}\hat{\rho}_{12}^{\dagger}\right\rangle + \left\langle \hat{\rho}_{12}\left(\Gamma_e\hat{\rho}_{12}^{\dagger}\right)\right\rangle \end{aligned}$$

$$
\begin{aligned}
&= \left\langle \frac{d}{dt}\rho_{11} \right\rangle_{\mathrm{NH}} + 2\Gamma_e\rho_{11} \\
&= \gamma_{21}\rho_{22} - \gamma_{10}\rho_{11} + 2\Gamma_e\rho_{11} \\
\left\langle \hat{F}_{12}^{\dagger}\hat{F}_{12} \right\rangle &= \gamma_{32}\rho_{33} - \gamma_{21}\rho_{33} + 2\Gamma_e\rho_{22} \\
\left\langle \hat{F}_{00}\hat{F}_{00} \right\rangle &= \left\langle \frac{d}{dt}\hat{\rho}_{00} \right\rangle_{\mathrm{NH}} - 2\left\langle \left(\gamma_{30}\hat{\rho}_{33} + \gamma_{10}\hat{\rho}_{11}\right)\hat{\rho}_{00} \right\rangle \\
\left\langle \hat{F}_{11}\hat{F}_{11} \right\rangle &= \gamma_{21}\rho_{22} + \gamma_{10}\rho_{11} \\
\left\langle \hat{F}_{22}\hat{F}_{22} \right\rangle &= \gamma_{32}\rho_{33} + \gamma_{32}\rho_{22} \\
\left\langle \hat{F}_{33}\hat{F}_{33} \right\rangle &= \gamma_{32}\rho_{33} + P_r\rho_{00}
\end{aligned} \tag{4}
$$

In order to work with temporal real-valued Maxwell equations, the first-order complex differential equation for ρ_{12} and F_{12} can be derived into a second-order real-valued differential equation:

$$
\begin{aligned}
&\frac{\partial^2 \mathrm{Re}\left(\rho_{12}\right)}{\partial t^2} + 2\Gamma_{\mathrm{e}}\frac{\partial \mathrm{Re}\left(\rho_{12}\right)}{\partial t} + \left(\omega_e^2 + \Gamma_e^2\right)\mathrm{Re}\left(\rho_{12}\right) \\
&= -\omega_e\frac{\Upsilon_e E}{\hbar}\left(\rho_{22} - \rho_{11}\right) - \left(\omega_e \,\mathrm{Im}\left(F_{12}\right) + \frac{\partial \mathrm{Re}\left(F_{12}\right)}{\partial t}\right)
\end{aligned} \tag{5}
$$

The real-valued diagonal elements of the density matrix stand with stochastic noise terms can be transformed as

$$
\begin{aligned}
\frac{\partial\rho_{00}}{\partial t} &= -P_r\rho_{00} + \gamma_{10}\rho_{11} + F_{00} \\
\frac{\partial\rho_{11}}{\partial t} &= -2\,\mathrm{Im}\left(\Omega_{12}\rho_{12}\right) + \gamma_{21}\rho_{22} - \gamma_{10}\rho_{11} + F_{11} \\
&= -\frac{2\Upsilon_e E}{\hbar\omega_e}\left(\frac{\partial \mathrm{Re}\left(\rho_{12}\right)}{\partial t} + \Gamma_e\,\mathrm{Re}\left(\rho_{12}\right)\right) \\
&\quad + \gamma_{21}\rho_{22} - \gamma_{10}\rho_{11} + F_{11} \\
\frac{\partial\rho_{22}}{\partial t} &= \frac{2\Upsilon_e E}{\hbar\omega_e}\left(\frac{\partial \mathrm{Re}\left(\rho_{12}\right)}{\partial t} + \Gamma_e\,\mathrm{Re}\left(\rho_{12}\right)\right) \\
&\quad + \gamma_{32}\rho_{33} - \gamma_{21}\rho_{22} + F_{22} \\
\frac{\partial\rho_{33}}{\partial t} &= P_r\rho_{00} - \gamma_{32}\rho_{33} + F_{33}
\end{aligned} \tag{6}
$$

Here P_r is a homogeneous pumping rate [30]. Eqs. 5,6 are derived under the assumption of $\rho_{00} + \rho_{11} + \rho_{22} + \rho_{33} = 1$. In a realistic 3D system, the macroscopical polarization $\mathbf{P}_e$ and the occupied densities N_i in state i are proportional to the microscopic values $\mathrm{Re}(\rho_{12})$ and ρ_{ii}. The proportionality factors to transform the microscope to the macroscope are depended on the density of the atoms in per unit volume. Therefore, the polarization densities of the emission transition $\mathbf{P}_e$ with Langevin noise terms driven by the local electric field obeys the following equation

$$
\begin{aligned}
\frac{\partial^2\mathbf{P}_e}{\partial t^2} = &-2\Gamma_e\frac{\partial\mathbf{P}_e}{\partial t} - \omega_e^2\mathbf{P}_e - \sigma_e\left(N_2 - N_1\right)\mathbf{E} \\
&- \kappa_e\left(\omega_e\,\mathrm{Im}\left(\mathbf{\Gamma}_{12}\right) + \frac{\partial \mathrm{Re}\left(\mathbf{\Gamma}_{12}\right)}{\partial t}\right)
\end{aligned} \tag{7}
$$

$\sigma_{e,a}$ are the phenomenological coupling constant of the local electric field to $\mathbf{P}_e$. κ_e is the proportionality factor to transform $\mathrm{Re}(\rho_{12})$ to the polarization density $\mathbf{P}_e$. The macroscopical noise term $\mathbf{\Gamma}_{12}$ is a complex number. The temporal evolution of the occupation numbers at each spatial point vary following the rate equations

$$
\begin{aligned}
\frac{\partial N_3}{\partial t} &= P_{\mathrm{r}}N_0 - \gamma_{32}N_3 + N_{\mathrm{v}}\Gamma_{33} \\
\frac{\partial N_2}{\partial t} &= \frac{1}{\hbar\omega_e}\left(\frac{\partial\mathbf{P}_e}{\partial t} + \Gamma_e\mathbf{P}_e\right)\cdot\mathbf{E} + \gamma_{32}N_3 - \gamma_{21}N_2 + N_{\mathrm{v}}\Gamma_{22} \\
\frac{\partial N_1}{\partial t} &= -\frac{1}{\hbar\omega_e}\left(\frac{\partial\mathbf{P}_e}{\partial t} + \Gamma_e\mathbf{P}_e\right)\cdot\mathbf{E} + \gamma_{21}N_2 - \gamma_{10}N_1 + N_{\mathrm{v}}\Gamma_{11} \\
\frac{\partial N_0}{\partial t} &= -P_{\mathrm{r}}N_0 + \gamma_{10}N_1 + N_{\mathrm{v}}\Gamma_{00}
\end{aligned} \tag{8}
$$

where Γ_{ii} are the real-value noise terms. In a typical four-level system $\gamma_{21} \ll \gamma_{32}$ and γ_{10}, and noise terms in 4 related to γ_{21} can be neglected. Then the noise terms in the emission polarization density equation and rate equations can be derived as

$$
\begin{aligned}
\Gamma_{12} &= \left(\mathrm{Re}\left(\xi_{12}\right) + i\,\mathrm{Im}\left(\xi_{12}\right)\right)\sqrt{\left\langle \hat{F}_{12}\hat{F}_{12}^{\dagger} \right\rangle N_{\mathrm{v}}} \\
&= \mathrm{Re}\left(\xi_{12}\right) + i\,\mathrm{Im}\left(\xi_{12}\right)\sqrt{\gamma_{32}N_3 + \left(2\Gamma_{\mathrm{e}} - \gamma_{21}\right)N_2} \\
\Gamma_{00} &= \xi_{10}\sqrt{\left\langle \hat{F}_{12}\hat{F}_{12}^{\dagger} \right\rangle N_{\mathrm{v}}} = \xi_{10}\sqrt{\gamma_{10}N_1} \\
\Gamma_{11} &= -\xi_{10}\sqrt{\gamma_{10}N_1} \\
\Gamma_{22} &= \xi_{32}\sqrt{\gamma_{32}N_3} \\
\Gamma_{33} &= -\xi_{32}\sqrt{\gamma_{32}N_3}
\end{aligned} \tag{9}
$$

here ξ_{ij} are random, Gaussian variables with zero mean fulfilling the two-time correlation and can be generated by the Ziggurate algorithm [31]. Equations (7)-(9), coupled to the Maxwell equations (1) provide the self-consistent Langevin Maxwell-Bloch approach to stimulated emission and spontaneous emission noise in semiconductor microdevices.

B. Numerical Implementation

In order to numerically solve the EM and semiclassical dynamics described in Eqs. (1), (7)-(9), the FDTD method is adopted. We extend the FDTD method and discretize the Maxwell's equations together with the equations for the semiconductor polarization and volume electron densities N_v. Maxwell's equations are approximated by the second-order center difference scheme so that both three dimensional space and time are discretized, the electric field components are set at the time step n while the magnetic field components are set at the time step $n + 1/2$, leading to second-order accurate for the spatial and temporal interleaving of the electromagnetic fields. The spatio-temporal dynamics in the form of polarization density in the semiconductor regime can be described by solving sets of auxiliary differential equations. The details and numerical implementations of the Maxwell-Bloch theory and FDTD algorithm are presented in [32]–[34]. Note that the noise terms

under the square root in (9) contain a time derivative. We adopt the Euler forward integration

$$\left.\frac{\partial(\xi\sqrt{\Phi})}{\partial t}\right|^{n+1} = \left(\xi^{n+1}\sqrt{\Phi^{n+1}} - \xi^{n}\sqrt{\Phi^{n}}\right)/\Delta t \tag{10}$$

where Φ indicates the term under the square root. The numerical stability of the Langevin Maxwell-Bloch system is subject to the Courant Friedrichs Lewy (CFL) condition due to the explicit nature of the iterated formula.To saving computing time and storage space, the initial condition of the four-level system is set as the saturated state, that is, the population number changes very slowly with time. By the initial condition, we do not need a pump process and a long-time decay for pump pulse. The population numbers at each level can be obtained as

$$\begin{aligned} N_3 &= \frac{N_v/\gamma_{32}}{1 + P_{\mathrm{r}}/\gamma_{32} + P_{\mathrm{r}}/\gamma_{21} + P_{\mathrm{r}}/\gamma_{10}} \\ N_2 &= \frac{N_v/\gamma_{21}}{1 + P_{\mathrm{r}}/\gamma_{32} + P_{\mathrm{r}}/\gamma_{21} + P_{\mathrm{r}}/\gamma_{10}} \\ N_1 &= \frac{N_v/\gamma_{10}}{1 + P_{\mathrm{r}}/\gamma_{32} + P_{\mathrm{r}}/\gamma_{21} + P_{\mathrm{r}}/\gamma_{10}} \\ N_0 &= \frac{N_v}{1 + P_{\mathrm{r}}/\gamma_{32} + P_{\mathrm{r}}/\gamma_{21} + P_{\mathrm{r}}/\gamma_{10}} \end{aligned} \tag{11}$$

In addition, considering the uncertainty principle, an initial tipping angle θ of the Bloch vector for the emission channel has to be assumed. The θ is a Gaussian distributed stochastic value centered at 0 with a deviation of $2/\sqrt{N_1 + N_2}$.

In the developed solver based on FDTD, the most computational-intensive work is for the FDTD iteration. Since the plasmonic nanodevices, such as metamaterials, are sub-wavelength nanostructures exhibiting a strong near-field enhancement. Simulations of them need a great number of grids to achieve a high spatial resolution. Meanwhile, the excited levels have characteristic lifetimes as long as a few milliseconds. Accordingly, due to the time step imposed by the ADE-FDTD method lower than 10^{-17} s for simulations in the optical frequency region, the FDTD iteration steps will be a huge number to reach the steady states of the levels populations. Thus, in the full-wave analysis of an active device with relatively large dimensions, a large number of meshes and time steps are required to ensure adequate accuracy. As a result, long CPU time with large iteration steps is required to guarantee the sufficient decay of the emission signals. This leads to the drastic increase in computation time and renders this approach not applicable as a practical tool for full-wave simulations on CPUs of today's desktop computers. To fix this problem, a parallel computing technique based on Compute Unified Device Architecture (CUDA) can be employed. Thanks to the localization nature of the FDTD method, we can divide the whole computational domain into several subdomains. A high efficient parallel code can then be achieved by implementing the FDTD code on a computer cluster with multi GPUs. The simulation domain is divided into several subdomains and each subdomain is assigned to a GPU. Each subdomain executes the same code in parallel and swaps the data at the interface at every time step. The data exchange between different processors or domains is carried out by using the message passing interface (MPI) library. At the subdomain boundaries, one additional layer of cells is allocated as a swap buffer. The flowchart of the subdomain is demonstrated in Fig. 1.

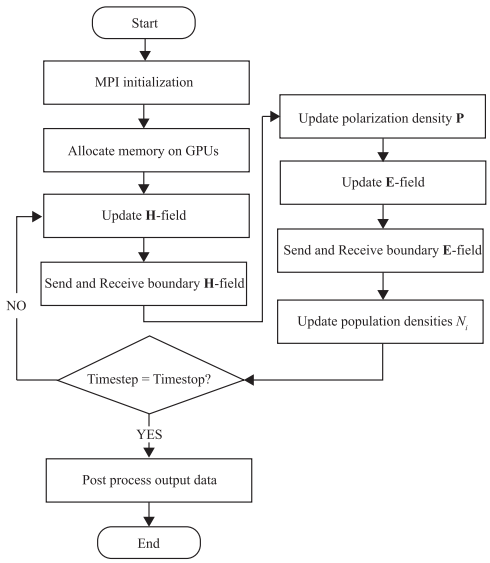

Fig. 1. Flow chart of the parallel FDTD algorithm.

C. Validation: Transition From Superfluorescence to Amplified Spontaneous Emission

In order to validate our numerical method, the Langevin Maxwell-Bloch equations are self-consistently solved with the FDTD method. We performed a validation case and compare it with previous experimental and numerical studies [22], [35]. As reported in previous work, superfluorescence (SF) from a KCl crystal can be disturbed by collisional dephasing induced by noise and transfer to amplified spontaneous emission (ASE). Andreasen *et al.* applied a model based on Maxwell-Bloch equations with pseudorandom noise terms to numerically study the interplay between noise and spatial propagation of light. We simulate the varied emission characters in a one-dimensional system and compare the results with the experimental and theoretical results. In this benchmark simulation, a set of parameters are adopted corresponding to the experiment. $1/\gamma_{21} = 76$ ns, $\omega_e = 2\pi \times 477 \times 10^{12}$ rad/s and Γ_e varies from $1/100$ ps^{-1} to $1/15$ ps^{-1} by changing temperature. The total excited ions $N_v = 3 \times 10^9$ are estimated in a 7 mm length super-oxide ions wire. The lifetimes $1/\gamma_{10}$ and $1/\gamma_{32}$ are chosen as $\gamma_{10} = \gamma_{32} = 0$ and the initial ions density are set to $N_2 = N_v$ so that the four-level system can be reduced to a two-level system. An initial random tipping angle of the Bloch vector in the emission transition dipole moment is needed to start the SF and the simulation start without external pumping, P_r is set to 0. By the given parameters, the time delay and pulse-width of the SF peak can be estimated as $\tau_r = 2.7$ ps and $\tau_d = 94$ ps leading to a minimum dephasing time $T_e = \sqrt{\tau_r \tau_d} = 15.9$ ps. Figure 1 shows the emitted field energy for different dephasing times

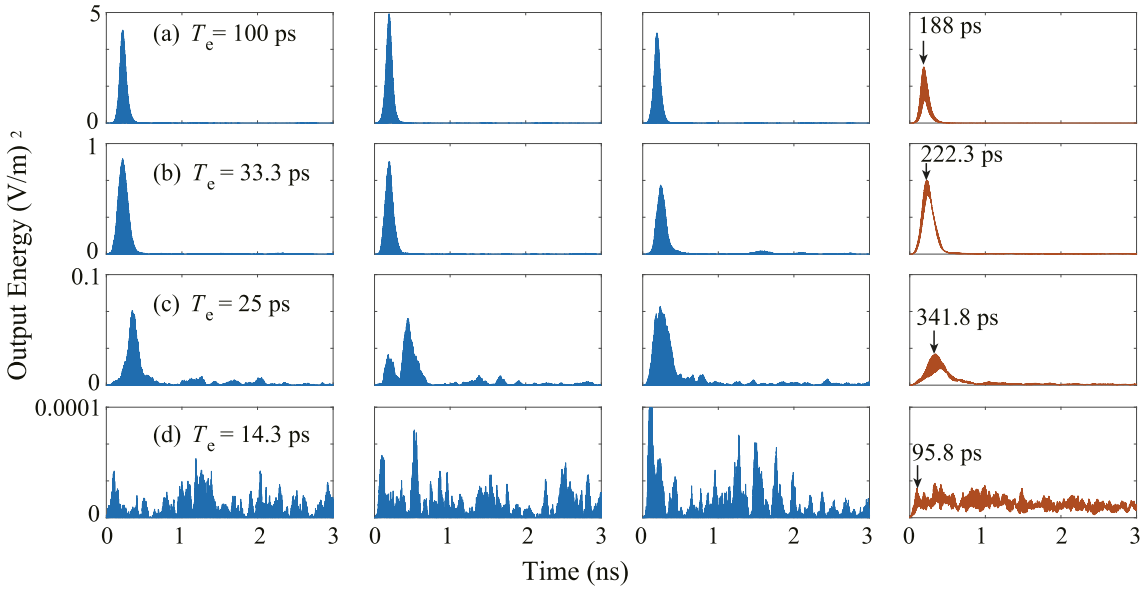

Fig. 2. Transition from SF to ASE in a 1D system as seen in the output EM energy for dephasing time: (a) $T_e = 100$ ps, (b) $T_e = 33.3$ ps, (c) $T_e = 25$ ps,and (d) $T_e = 14.3$ ps. The left three columns show three random results. The last column shows the average over 20 random realizations. The arrows indicate the delay time of emission pulse.

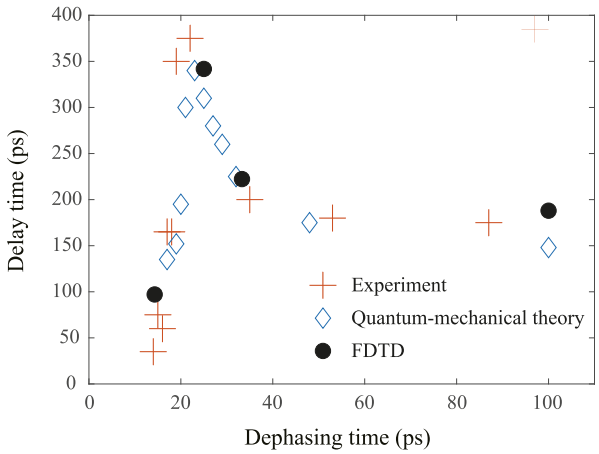

Fig. 3. Comparisons of emission pulse delay time of our simulated results (black solid circles) with quantum-mechanical calculation results (blue diamonds) and experimental results (red crosses) taken from [36].

T_e. When $T_e = 100$ ps $> \tau_{\rm d}$ the collective emission characteristic SF can be observed in Figure 2 a; Since the SF is the collective radiation from an ensemble of population inverted but incoherent atoms which critically depends on noise. The noise can significantly disturb the emission character from SF to incoherent ASE. Thus by reducing the dephasing times, for $T_e = 33.3$ ps and $T_e = 25$ ps, we find SF with moderate and strong noise modulations; and for $T_e = 14.3$ ps $< \tau_{\rm r}$, the value of dephasing reaches the critical value 15.9 ps which will prevent the collective emission. Indeed, instead of SF, ASE is found as expected. Figure 3 compares the delay times simulated by our method to previous experimental results and results obtained by full quantum-mechanical theory [36]. Our results agree well with the experimental and numerical results.

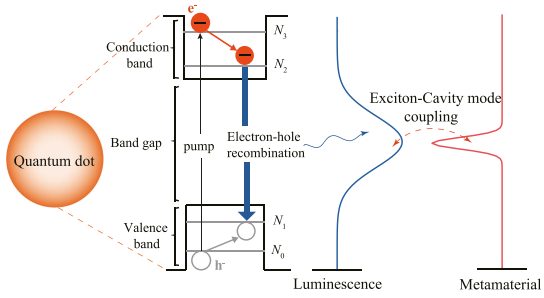

Fig. 4. Schematic illustration of controlling and enhancing emission from QD with metamaterial nanostructures.

III. Results and Discussion

Controlling the emission spectra and characteristics of semiconductor QD is an important subject for laser, biomarkers in biotechnology, quantum information, light-emitting devices, etc. Recent progress in nanofabrication technologies enabled tuning and the manipulation of fluorescence by introducing metamaterials. Figure 4 shows a schematic of the energy level diagram in the metamaterials including the QDs, which are coupled with cavity modes in the metamaterials. Due to the coupling, the interplay between the metamaterials and the QDs is incorporated. In this section, we numerically investigate manipulation of photoluminescence of QDs by plasmonic and all-dielectric metasurfaces. The numerical results agree well with experimental results and represent an important step in the development and understanding of active metamaterials devices.

A. Spectrum Modulation of QDs Luminescence in Plasmonic Metasurface

The interaction between light and metal nanostructures offers a variety of functions and properties by surface plasmon resonance (SPR). SPR opens up opportunities for controlling

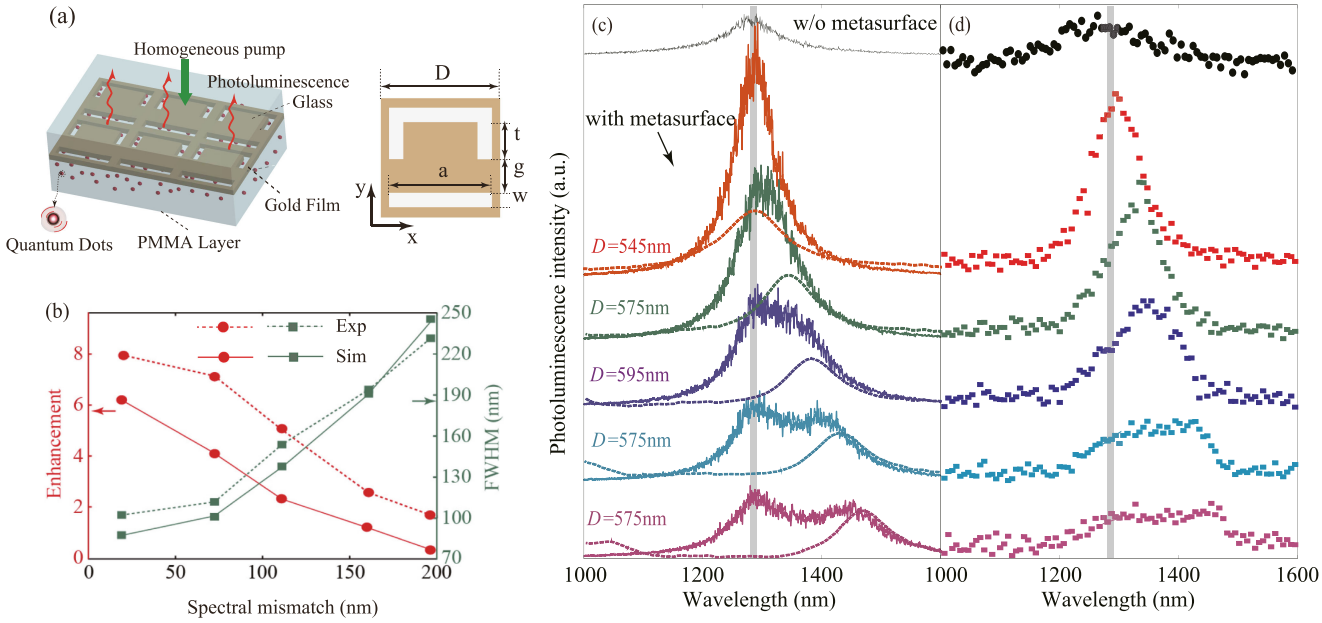

Fig. 5. (a) Configuration of the metasurface functionalized with QDs. (b) Comparison of the PL peak intensity enhancement and FWHM of the active metasurface to previous results obtained experimentally [39]. The enhancement is referenced to the PL peak intensity without metasurface. (c) Simulated PL spectra of the QDs without (black) and with metasurface (colored) for different unit size. The dashed lines show the absorption spectra of the metasurfaces. (d) Experimental results adopted from [39] and the solid lines indicate our simulated results.

light confinement at a deep subwavelength scale. The strong local field enhancement effect can provide a cavity for shaping and tuning light emission from optically active materials. It has been experimentally reported that extraction and enhancement of PL dynamics from QDs can be attempted by introducing plasmonics [37], [38]. Here, we numerically consider the plasmon-QD coupling system presented by K. Tanaka [39]. Figure 5 a shows the plasmonic metasurface combined with lead sulfide (PbS) QDs. The 50 nm thickness metasurface consists of complementary split-ring slits arrays and sandwiched between a 180 nm thick polymethylmethacrylate (PMMA) layer doped with QDs and a glass substrate. The detailed feature sizes of the meta-atom are indicated in the inset of Figure 5 a. The permittivity of the gold metasurface is characterized by a Drude model: $\epsilon(\omega) = \epsilon_\infty - \omega_p^2/(\omega^2 + i\omega\gamma)$, where $\epsilon_\infty = 9$ is the background permittivity, $\omega_p = 2\pi \times 2.184 \times 10^{15}\,\mathrm{rad/s}$ is the plasmon frequency, and $\gamma = 5.6 \times 10^{12}\,\mathrm{s}^{-1}$ denotes the phenomenological damping constant. The parameters of the QDs/PMMA can get from the experiments. We set the values of the QDs/PMMA active layer as $\omega_p = 2\pi \times 2.05 \times 10^{14}$ rad/s and $\Gamma_e = 1/9.69\ \mathrm{fs}^{-1}$. The QD can be characterized by a three-level atomic system. By setting $\gamma_{10} = 0$ and $N_1 = N_v$ as the ground state, the four-level system will be reduced to a three-level atomic system. A total density of $N_v = 5 \times 10^{23}\ \mathrm{m}^{-3}$, lifetimes $1/\gamma_{10} = 1/\gamma_{32} = 50$ fs and $1/\gamma_{21} = 50$ ns, and coupling strength σ_e are assumed here.

To systematically study the interplay between the spectral position of the QDs and the plasmonic cavity mode spectrum. Five different resonant frequencies metasurface by changing unit cell size ranging from D = 545 nm to 645 nm are considered. To calculate the PL dynamics, multi-monitors are placed above the glass substrate to record the emitted energy from the pumped active plasmonic system. Figure 5 c and d show the simulated and experimental measured PL spectra of the coupling systems with and without plasmonic metasurface. One can see that the QDs PL intensity characteristics drastically changed by introducing the plasmonic metasurfaces. For the case of D = 545 nm, the absorption spectrum peak for y polarization shows a collective resonance of the metasurface around 1300 nm (see the absorption spectrum plotted by the red dashed line). The spectral match of the metasurface resonance and the QD emission wavelength leads to about 7 times enhancement of the PL peak intensity as well as decreases the FWHM of the PL peak from ∼180 nm without the metasurface to 100 nm. The PL spectrum becomes weaker and broader when the metasurface resonance is redshifted by increasing the unit cell size from D = 545 nm to 645 nm. Simultaneously, the PL peak is redshifted, for a large mismatch D ≥ 620 nm, the emission spectrum becomes distorted with two peaks. The PL spectrum peak intensity and FWHM as a function of the spectral mismatch are summarized in Figure 5 b. We note that the value of PL enhancement factor and the spectral feature are in good agreement with those of experimental results taken from [39].

B. Manipulating Light Emission by all-Dielectric Metasurface

Metasurfaces consist of dielectric materials with negligible ohmic loss is a promising way to circumvent the dissipative loss involved with plasmonic metamaterials. Recently, the use of all-dielectric designs, such as all-dielectric antenna and metamaterials, has attracted intense interest. As compared to the plasmonic metal materials, the dielectric materials such as silicon or germanium own weaker absorption coefficients. Hence, the dielectric microcavities such as dielectric photonic crystals,

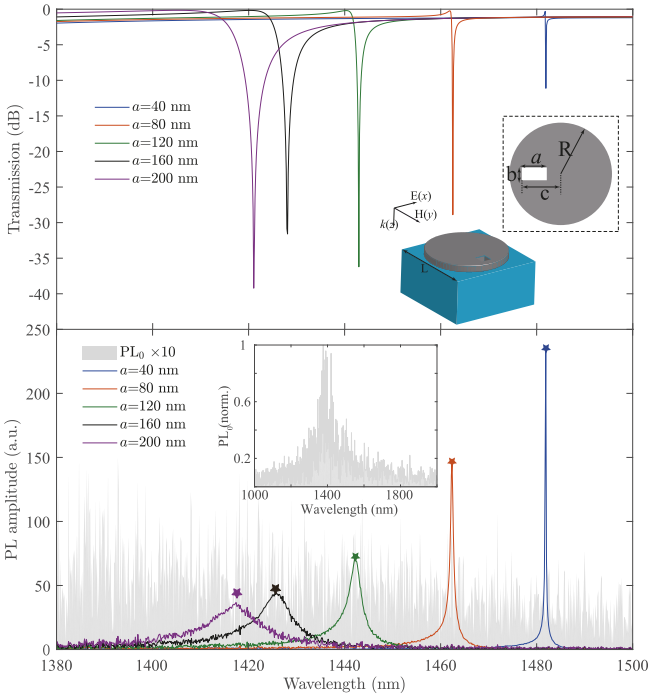

Fig. 6. Relative transmission (top) and PL spectra (bottom) of the active metasurfaces with different slot configurations. As the slot size gets larger, the PL spectrum gets weaker, broader, and noise. PL spectrum of QDs in a pattern-free structure is plotted by the gray area and magnified by 10 times. The star points indicate the Purcell factors of different a at the corresponding wavelengths.

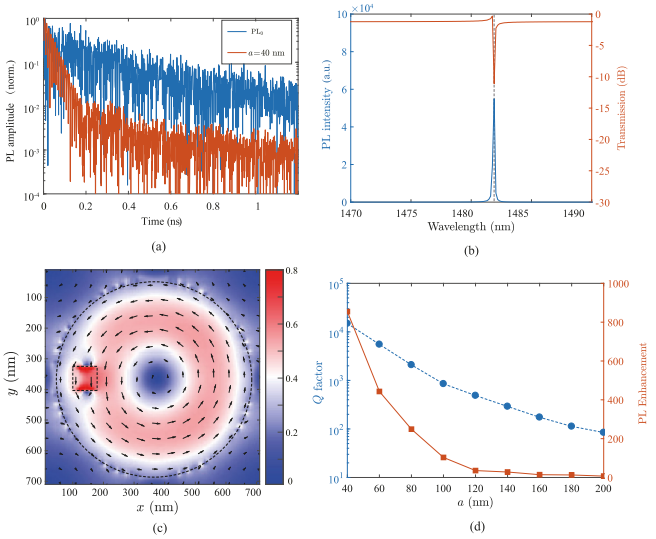

Fig. 7. (a) shows the time trace of the PL for $a = 40\ nm$ and the pattern-free reference case. (b) Relative transmission and PL spectra of the active metasurface with slot size $a = 40\ nm$. (c) PL near field distribution with vector arrows of a meta-atom.(d) Q-factor and PL controlled by the slot size a. The Enhancement is normalized to the PL peak intensity of the unpatterned case.

trapped mode microresonators, or planar concentrators can feature extremely high Q-factors. These all-dielectric micro designs have already been utilized for emission shaping, enhancement, and light extraction applications. In this subsection, with the help of the proposed method, we investigate how all-dielectric metasurfaces affect the emission properties of an active medium.

To achieve a high Q-factor metasurface, an all-dielectric metasurface that can support "dark" mode or trapped mode has been experimentally studied [40], [41], [42], [43], [44]. Here, an all-dielectric metasurface consisting of meta-atom supporting "dark" mode is utilized for investigating the interplays between all-dielectric metasurfaces and Ge QDs [42], [44]. The all-dielectric metasurface consists of two basic parts: a non-radiative resonator and an appropriate scatterer. The "dark" resonator is comprised of a silicon disk ($\epsilon \approx 12$, R $= 320$ nm, with thickness 160 nm shown in Figure 6) placed on a silica substrate ($\epsilon \approx 2.25$) and the unit cell is periodically repeated in the x and y directions to form a metasurface. To achieve a "dark" Mie mode from the homogeneous disk, we introduce an off-centered slot (a varies from 40 to 200 nm, b $= 80$ nm, c $= 240$ nm) along y direction in the disk creating symmetry-broken in the meta-atom. The slot serves to the energy exchange from the external field into the nonradiative magnetic dipole mode, resulting in a circulating electric field. The Q-factor of the "dark" mode is limited by the asymmetry rate of the unit cell.

To explore the response property of the "dark" mode, we first calculate the transmission spectra of the metasurface with different etched slot sizes. By changing the slot size, the transmission spectrum for x polarization of the metasurface dramatically changed as shown in the upper portion of Figure 6. Then we investigate the mechanism of emission characteristic modulation by the all-dielectric metasurface. We assume the silicon is doped with QDs. The emission frequency and emission dephasing rate of the QD are set as 1450 nm and 100 nm, and the other parameters are set the same as the previous subsection. The PL spectra for different metasurface are presented at the bottom of Figure 6. Indeed, the Q-factors of the "dark" resonator decrease monotonously as the off-centred slot becomes larger. After pumping the QDs embedded metasurface, the presence of the etched slot drastically changes the resonator from non-radiative to radiative and leads to a multi-fold enhancement of PL peak intensity. The shaded gray area indicates the PL spectrum of QDs embedded in a metasurface without the etched slot as a reference case. For a specifically $a = 40$ nm, the PL time traces in the Figure 7 b show that the patterned metasurface has a fast PL decay curve, and the PL and transmission spectra are shown in Figure 7 a. The field intensity profile and field vector distributions of the near field spontaneous emission are shown in Figure 7 c indicating a magnetic dipole mode. The PL spectrum of the active metasurface functionalized with the "dark" resonator is shown in Figure 7 d. Notice that the PL intensity peak position is dominated by the resonant peak and agrees well with the relative transmission spectrum dip. When the metasurface resonance is blue-shifted by increasing the slot size from 40 nm to 200 nm, the PL spectrum is broadened and the peak shifted following the resonance of the "dark" mode. The PL intensity enhancement factor (define as the ratio of the peak intensity to the reference PL intensity at the same wavelength) reaches high values of about 845, 210, 23, 11, and 3 for slot sizes 40, 80, 120, 160, and 200 nm, respectively. The PL enhancement rate of the active devices can be estimated by the Purcell factor, the calculated Purcell factors at the wavelength of the emission spectra peak for different configurations are marked

(star points) in the bottom figure of Fig. 6. We observe a good agreement between the Purcell factor and PL enhancement. The Q-factor and Purcell factor in the active devices are calculated by the method presented in the Appendix section. In addition, our numerical observations are in good agreement with the experimental results in [42], [44].

IV. Conclusion

In summary, we proposed a semiclassical model for simulating spontaneous emissions and the coherent emission dynamics of active metasurfaces based on the Langevin theory and rate equations of a multi-level quantum system. Comparing with previous works, a significant advantage of our nonperturbative numerical approach is that the derived initial condition of a multi-level gain system can save computing time and storage space. A parallel ADE-FDTD algorithm based on the CUDA technique was developed to solve the multiphysical model self-consistently. The proposed model and numerical method were validated against previous theoretical and experimental results, which are valid for both plasmonic and extremely high Q-factor all-dielectric metamaterial based active nanodevices. The proposed semiclassical method offers a deep insight into the mechanism of the cavity quantum electrodynamics in active metamaterials and reveals a new approach for developing functional active metasurfaces.

Appendix A
Purcell Factor Calculation

The PL enhancement rate of a spontaneous emission in a nanocavity can be predicted by the Purcell factor

$$F_p = \frac{3}{4\pi^2}\left(\frac{\lambda}{n}\right)^3 \frac{Q}{V} \tag{12}$$

where λ/n is the wavelength within the cavity materials of refractive index n. Q is the quality factor and V indicates the cavity mode volume. For the calculation of a high Q-factor cavity based on all-dielectric metamaterial in the time-domain simulation, the electromagnetic power cannot decay rapidly, and cannot evaluate the Q-factor from the resonant spectrum by the definition of Q-factor in 13, because the FWHM of resonance is changed by the simulation time.

$$Q = \frac{\omega_0}{FWHM} \tag{13}$$

In this case, the Q-factor can be calculate by the slope of the decaying field. The electric field of the resonance can be described by

$$E(t) = e^{i\omega_0 t - \gamma t} \Leftrightarrow |E(\omega))|^2 = \frac{1}{\gamma^2 + (\omega - \omega_0)^2} \tag{14}$$

where γ is the decay constant due to the radiation and dissipation of the cavity. By taking the log of $E(t)$, the exponentially decaying field can be described by a linear function

$$\log_{10}(|E(t))|) = -\frac{\omega_0 t}{2\gamma}\log_{10}(e) = mt \tag{15}$$

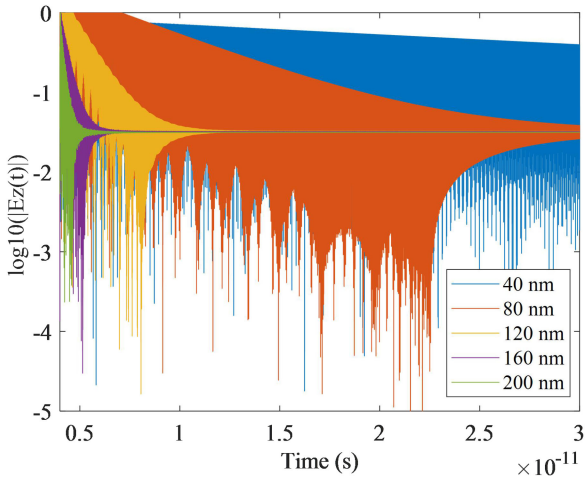

Fig. 8. Logplot the decay of electric field of the active device with different slot size in Fig. 6.

where m is the slope of the linear function. From 13, the half maximum and maximum values can be obtained at $\omega_0 + \gamma, \omega_0 - \gamma$ and ω_0, respectively. By substituting the half max frequencies into 13, we can get the relation between γ and Q

$$\gamma = \frac{\omega_0}{2Q} \tag{16}$$

Substituting 16 into 15, we get

$$Q = \frac{-\omega_0 \log_{10}(e)}{2\tilde{}m} \tag{17}$$

Instead of using randomly distributed dipole sources to excited the cavity modes, we pumped the active devices with high pumping power let the devices lasing at a chosen mode. After the devices lasing, the pumping source disabled and the lasing field will be exponential decay. Then we can calculated the Q-factor of the all-dielelctric metamaterial based active devices as shown in Fig. 8.

The mode volume V calculated by:

$$V(\omega) = \frac{\int_V \epsilon(\omega, r)\,|E(\omega, r)|^2\,\tilde{}\,d^3r}{max\,(\epsilon(\omega, r)|E(\omega, r)|^2)} \tag{18}$$

where $\epsilon(\omega, r)$ is the material permittivity at position r

References

[1] N. I. Zheludev, S. L. Prosvirnin, N. Papasimakis, and V. A. Fedotov, "Lasing spaser," *Nat. Photon.*, vol. 2, pp. 351–354, 2008.
[2] M. Decker *et al.*, "Dual-channel spontaneous emission of quantum dots in magnetic metamaterials," *Nat. Commun.*, vol. 4, 2013, Art. no. 20411723.
[3] W. Zhou *et al.*, "Lasing action in strongly coupled plasmonic nanocavity arrays," *Nat. Nanotechnol.*, vol. 8, pp. 506–511, 2013.
[4] S. Luo *et al.*, "Controlling fluorescence emission with split-ring-resonator-based plasmonic metasurfaces," *Laser Photon. Rev.*, vol. 11, 2017, Art. no. 1600299.
[5] P. Song *et al.*, "Three-level spaser for next-generation luminescent nanoprobe," *Sci. Adv.*, vol. 4, 2018, Art. no. 8, eaat0292.
[6] V. I. Klimov *et al.*, "Single-exciton optical gain in semiconductor nanocrystals," *Nature*, vol. 447, pp. 441–446, 2007.
[7] F. Jahnke and S. W. Koch, "Many-body theory for semiconductor microcavity lasers," *Phys. Rev. A.*, vol. 52, pp. 1712–1727, 1995.
[8] W. C. Chew, W. E. I. Sha, and Q. Dai, "Green's dyadic, spectral function, local density of states, and fluctuation dissipation theorem," *Prog. Electromagn. Res.* vol. 166, pp. 147–165, 2019.

[9] H. F. Hofmann and O. Hess, "Quantum Maxwell-Bloch equations for spatially inhomogeneous semiconductor lasers," *Phys. Rev. A. - At Mol. Opt. Phys*., vol. 59, pp. 2342–2358, 1999.

[10] M. Kira *et al.*, "Quantum theory of nonlinear semiconductor microcavity luminescence explaining ..Boser.. experiments," *Phys. Rev. Lett*., vol. 79, pp. 5170–5173, 1997.

[11] M. Kira, F. Jahnke, and S. W. Koch, "Microscopic Theory of excitonic signatures in semiconductor photoluminescence," *Phys. Rev. Lett*., vol. 81, pp. 3263–3266, 1998.

[12] M. Kira, F. Jahnke, and S. W. Koch, "Quantum theory of secondary emission in optically excited semiconductor quantum wells," *Phys. Rev. Lett*., vol. 82, pp. 3544–3547, 1999.

[13] A. Taflove, S. C. Hagness, and M. Piket-May, in: *Electr. Eng. Handb.*, pp. 629–670, 2005.

[14] A. Capua, O. Karni, and G. Eisenstein, "A Finite-difference time-domain model for quantum-dot lasers and amplifiers in the Maxwell."Schrdinger framework," *IEEE J. Sel. Top. Quantum Electron*., vol. 19, 2013, Art. no. 1900410.

[15] J. Bai, H. Wang, Q. Wang, D. Zhou, K. Q. Le, and B. Wang, "Coherent pulse progression of mid-infrared quantum-cascade lasers under group-velocity dispersion and self-Phase," *IEEE J. Quantum Electron*., vol. 52, 2016, Art. no. 2300106.

[16] S. Ahmad, "Quantum analysis of plasmonic coupling between quantum dots and nanoparticles," *Phys. Rev. A*., vol. 94, 2016, Art. no. 043819.

[17] K. Kalna, C. Y. L. Cheung, I. Pierce, and K. A. Shore, "Self-consistent analysis of carrier."transport and carrier."capture dynamics in quantum cascade intersubband semiconductor lasers," *IEEE Trans. Microw. Theory Tech*. vol. 48, pp. 639–644, 2000.

[18] C. M. Bowden, and G. P. Agrawal, "Maxwell-Bloch formulation for semiconductors: Effects of coherent Coulomb exchange," *Phys. Rev. A*., vol. 51, pp. 4132–4139, 1995.

[19] H. Duan, W. Fang, W. Yin, E. Li, and W. Chen, "Computational investigation of nanoscale semiconductor devices and optoelectronic devices from the electromagnetics and quantum perspectives by the finite difference time domain method," *Prog. Electromagn. Res*., vol. 170, pp. 63–78, 2021.

[20] M. Lax and W. H. Louisell, "Quantum noise. XII. Density-operator treatment of field and population fluctuations," *Phys. Rev*. vol. 185, pp. 568–591, 1969.

[21] G. M. Slavcheva, J. M. Arnold, and R. W. Ziolkowski, "FDTD simulation of the nonlinear gain dynamics in active optical waveguides and semiconductor microcavities," *IEEE J. Sel. Top. Quantum Electron*. vol. 10, pp. 1052–1062, 2004.

[22] J. Andreasen and H. Cao, "Finite-difference time-domain dormulation of stochastic noise in nacroscopic atomic systems," *J. Light. Technol*., vol. 27, pp. 4530–4535, 2009.

[23] A. Pusch, S. Wuestner, J. M. Hamm, K. L. Tsakmakidis, and O. Hess, "Coherent amplification and noise in gain-enhanced nanoplasmonic metamaterials: A Maxwell-Bloch Langevin approach," *ACS Nano*, vol. 6, pp. 2420–2431, 2012.

[24] A. Fang, T. Koschny, and C. M. Soukoulis, "Lasing in metamaterial nanostructures," *J. Opt. A. Pure Appl. Opt*. vol. 12, 2010.

[25] A. Fang, Z. Huang, T. Koschny, and C. M. Soukoulis, "Overcoming the losses of a split ring resonator array with gain," *Opt. Exp.* vol. 19, 2011, Art. no. 12688

[26] Z. Huang, T. Koschny, and C. M. Soukoulis, "Theory of pump-probe experiments of metallic metamaterials coupled to a gain medium," *Phys. Rev. Lett*., vol. 108, 2012, Art. no. 187402.

[27] W. E. I. Sha, A. Y. Liu, and W. C. Chew, "Dissipative quantum electromagnetics," *IEEE J. Multiscale Multiphys. Comput. Tech*., vol. 3, pp. 198–213, 2018.

[28] W. C. Chew, W. E. I. Sha, and Q. I. Dai, "Green's dyadic, spectral Function, local density of states, and fluctuation dissipation theorem," *Prog. Electromagn. Res*. vol. 166, pp. 147–165, 2019.

[29] M. Fang, Z. Huang, T. Koschny, and C. M. Soukoulis, "Electrodynamic modeling of quantum dot luminescence in plasmonic metamaterials," *ACS Photon.*, vol. 3, pp. 558–563, 2016.

[30] For a Thin Gain Slab Pumped by a Plane Wave, the Pumping Rate is Equivalent to the Pump Intensity. The Pump Power Density is Equal to $\hbar\omega_e P_r N_0$, and the Pump Intensity $I_{pump} = (Pumppower)/(surfaceArea) = \hbar\omega_e P_r N_0 (volume)/(surfaceArea) = \hbar\omega_e P_r N_0 \tilde{} d$; *here* d *is the thickness of the gain slab*.

[31] G. Marsaglia and W. W. Tsang, "The Ziggurat method for generating random variables," *J. Statist. Softw*. vol. 5, pp. 1–7, 2000.

[32] S. Wuestner, A. Pusch, K. L. Tsakmakidis, J. M. Hamm, and O. Hess, "Gain and plasmon dynamics in active negative-index metamaterials," *Philos. Trans. R. Soc. A. Math. Phys. Eng. Sci*. vol. 369, pp. 3525–3550, 2011.

[33] Q. Chen, M. Katsurai, and P. H. Aoyagi, "An FDTD formulation for dispersive media using a current density," *IEEE Trans. Antennas Propag*., vol. 46, pp. 1739–1746, 1998.

[34] Z. Huang, L. Shi, Z. Huang, and Z. Sun, "A theoretical extension of AH FDTD method and applications in various physical fields," *IEEE J. Multiscale Multiphys. Comput. Tech*., vol. 3, pp. 312–318, 2018.

[35] M. S. Malcuit, J. J. Maki, D. J. Simkin, and R. W. Boyd, "Transition from superfluorescence to amplified spontaneous emission," *Phys. Rev. Lett*., vol. 59, pp. 1189–1192, 1987.

[36] J. J. Maki, M. S. Malcuit, M. G. Raymer, R. W. Boyd, and P. D. Drummond, "Influence of collisional dephasing processes on superfluorescence," *Phys. Rev. A*., vol. 40, pp. 5135–5142, 1989

[37] S. A. Aljunid, E. A. Chan, G. Adamo, M. Ducloy, D. Wilkowski, and N. I. Zheludev, "Atomic response in the near-field of nanostructured plasmonic metamaterial," *Nano Lett*., vol. 16, pp. 3137–3141, 2016.

[38] G. M. Akselrod, M. C. Weidman, Y. Li, C. Argyropoulos, W. A. Tisdale, and M. H. Mikkelsen, "Efficient nanosecond photoluminescence from infrared PbS quantum dots coupled to plasmonic nanoantennas," *ACS Photon.*, vol. 3, pp. 1741–1746, 2016.

[39] K. Tanaka, E. Plum, J. Y. Ou, T. Uchino, and N. I. Zheludev, "Multifold enhancement of quantum dot luminescence in plasmonic metamaterials," *Phys. Rev. Lett*. vol. 105,2010, Art. no. 227403.

[40] I. Staude *et al.*, "Shaping photoluminescence spectra with magnetoelectric resonances in all-dielectric nanoparticles," *ACS Photon.*, vol. 2, pp. 172–177, 2015.

[41] A. Jain, P. Moitra, T. Koschny, J. Valentine, and C. M. Soukoulis, "Electric and magnetic response in dielectric dark states for low loss subwavelength optical meta atoms," *Adv. Opt. Mater*., vol. 3, pp. 1431–1438, 2015.

[42] S. Yuan *et al.*, "Strong photoluminescence enhancement in all-dielectric Fano metasurface with high quality factor," *ACS Nano*, vol. 11, pp. 10704–10711, 2017.

[43] S. Liu *et al.*, "Light-emitting metasurfaces: simultaneous control of spontaneous emission and far-field radiation," *Nano Lett*., vol. 8, pp. 6906–6914, 2018.

[44] C. Cui *et al.*, "Multiple Fano resonances in symmetry-breaking silicon metasurface for manipulating light emission," *ACS Photon.*, vol. 5, pp. 4074–4080, 2018.

Ming Fang received the Ph.D. degree from Anhui University, Hefei, China, in 2018. From January 2016 to January 2018, he was a Visiting Scholar with Iowa State University, Ames, IA, USA. From March 2015 to August 2015, he was a Research Assistant with the Department of Electrical and Electronic Engineering, University of Hong Kong, Hong Kong. His research interests include multiphysics modeling with time-domain numerical methods, metamaterials, and nonlinear optics.

Zhixiang Huang (Senior Member, IEEE) was born in Anhui, China, in 1979. He received the B.S. and Ph.D. degrees from Anhui University, Hefei, China, in 2002 and 2007, respectively. From 2010 to 2011, he was a Visiting Scholar with Iowa State University, Ames, IA, USA. His research interests include time-domain numerical methods, metamaterial, and active metamaterials.

Wei E. I. Sha (Senior Member, IEEE) received the B.S. and Ph.D. degrees in electronic engineering from Anhui University, Hefei, China, in 2003 and 2008, respectively. From July 2008 to July 2017, he was a Postdoctoral Research Fellow and then a Research Assistant Professor with the Department of Electrical and Electronic Engineering, University of Hong Kong, Hong Kong. From March 2018 to March 2019, he was with University College London, London, U.K., as a Marie Sklodowska Curie Individual Fellow. In October 2017, he joined the College of Information Science and Electronic Engineering, Zhejiang University, Hangzhou, China, where he is currently a tenure tracked Assistant Professor.

Costas M. Soukoulis received the B.Sc. degree from the University of Athens, in 1974 and the Ph.D. degree in physics from the University of Chicago, Chicago, IL, USA, in 1978, under the supervision of Kathryn Liebermann Levin. He is currently a Senior Scientist with Ames Laboratory, Ames, IA, USA, and a Distinguished Professor of physics emeritus with Iowa State University, Ames, IA, USA. From 1978 to 1981, he was with the Physics Department, University of Virginia, Charlottesville, VA, USA. From 1981 to 1984, he spent 3 years with Exxon Research and Engineering Co., and since 1984, he has been with Iowa State University and Ames Laboratory. From 2001 to 2011, he was a part-time Professor with the Department of Materials Science and Technology, University of Crete, Greece, and since 1984, he has been an Associated Member of IESL-FORTH at Heraklion, Crete, Greece. He is a Fellow of OSA, AAAS, APS.